4.1. Materials.

Ferrous chloride tetrahydrate (>99%), Iron (III) acetylacetonate (>97%), Benzyl ether (98%), 1-octadecene (90%), Oleyl amine (70%), (3-Carboxypropyl) triphenylphosphonium bromide (98%), Polyethelenimine branched (Mol. Wt. 25000g/mol) and florescamine (99%) were purchased from Sigma Aldrich, USA. Gadolinium chloride hexahydrate (99.99%) was procured from Global Nanotech, India. Gadolinium acetylacetonate (99.9%) was purchased from Alfa Aesar, USA. Oleic acid (>65%) was purchased from Merck, India. Diphenyl ether (98%), Folic Acid (Biochemistry grade) and sodium borohydrate (>98%) were procured from HiMedia, India. Polyvinyl alcohol (Mol wt.6000g/mol) was procured from Arcos Organics, USA. Diethylene glycol (>99.5%) and tetraethylene glycol (95%) were obtained from TCI chemicals, Japan. 1-(3-dimethylaminopropyl)-3-ethylcarbodiimide hydrochloride (synthesis grade) and N-hydroxysuccinimide (98%) were purchased from Spectrochem, India. Ferric chloride hexahydrate (99%), sodium hydroxide (97%), Hydrochloric acid (37.5%), tannic acid(AR), Potassium hydroxide (AR), citric acid anhydrous (99%), triethylene glycol (98%) were procured from Loba Chemie, India. Acetone, Toluene, Dimethyl sulphoxide and isopropyl alcohol (AR grade) were purchased from Rankem, India. Polylactide co glycolide (PLGA 50:50 acid terminated, Mol wt. 7000-17000, Resomer RG 502H) was obtained as gift sample from Evonik, India.

4.2. Screening of method for synthesis of Gadolinium doped Iron oxide nanoparticles (metallic core).

For the synthesis of the metal core consisting of Gd doped iron oxide nanoparticles various methods were attempted and most suitable method was selected based on feasibility, ease of synthesis and control on particle size.

4.2.1. Co-precipitation method.

4.2.1.1. Procedure .

In this method, the iron precursors namely ferrous chloride tetrahydrate and ferrous chloride hexahydrate were taken in the ratio of 1:2 (Fe^{+2}/Fe^{+3}) and were dissolved in 2N hydrochloric acid and the Gadolinium precursor was also dissolved in the same. The iron and gadolinium precursor were mixed resulting in 5 ml of the precursor solution which was filled in a syringe with 26 gauze needle. The precursor solution was added drop wise into the 3N sodium hydroxide solution which was kept on stirring at 1000 rpm and at 90°C using magnetic stirrer 1MLH, Remi, India. After addition of precursors, the stirring was continued for 1 hour after which the brownish black precipitate was separated using a bar magnet and washed twice with deionised water (1-4).

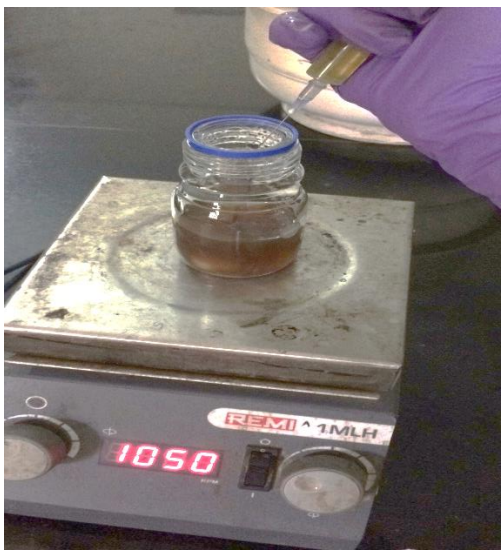

Figure 4.1: Co-precipitation synthesis process.

4.2.2. Borohydride reduction.

4.2.2.1. Procedure.

This synthesis is based on the reduction reaction of sodium borohydride on the chloride precursors. The iron and gadolinium precursors were dissolved in deionised water in ratio of 1:1 using 0.5mM of the each precursors in 10 ml deionised water and the precursor solution was filled in syringe with 26 gauze needle. In a 25 ml beaker, 10 ml of 4mM solution of sodium borohydride was prepared freshly in deionised water and kept on stirring in an ice bath at 1000 rpm using magnetic stirrer, 1MLH, Remi, India. The precursor solution was injected rapidly into the borohydride solution resulting in instant blackish precipitate and rapid evolution of hydrogen gas. The blackish precipitate was separated using a bar magnet and washed twice with deionised water and particle size was determined (5-8).

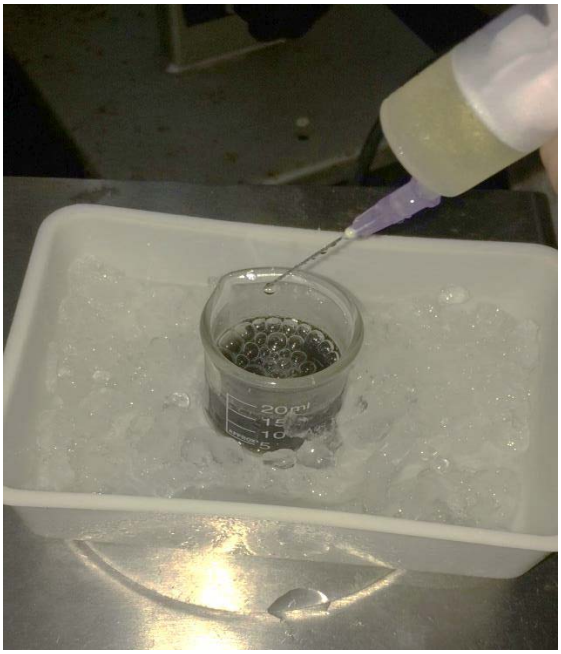

Figure 4.2: Synthesis by borohydride reduction.

4.2.3. Green synthesis (Tannin synthesis).

4.2.3.1. Procedure.

Tannins are class of phytochemicals which are non-toxic and biodegradable and can be used reducing agents for synthesis of metal nanoparticles.

For the synthesis the metal precursors of iron and gadolinium were taken in same ratio, while maintaining the 1:2 (Fe^{+2}/Fe^{+3}) internal ratio for iron precursors in 50ml deionised water and were kept on stirring at 1000 rpm at room temperature using a magnetic stirrer 1MLH, Remi, India. In another beaker, tannic acid solution (1mg/ml) was prepared from which it was added in the increments of 0.5 ml to the precursor solution till dark colour was observed. The particle size was measured after dark colour was observed (9).

4.2.4. Determination of degradation temperature of precursors for solvothermal and polyol process.

For determination of degradation temperature of iron acetylacetonate and gadolinium acetylacetonate hydrate differential scanning calorimeter was performed. The precursors were subjected to temperatures 30-300°C with ramping of 10°C/min under inert atmosphere and the thermal changes were recorded using Differential Scanning Calorimeter, DSC-60, Shimadzu, Japan (10).

4.2.5. Solvothermal method.

4.2.5.1. Procedure.

The iron and gadolinium precursors were loaded in 1:1 molar ratio along with 20 ml high boiling point solvent and surfactant in three necked RBF with attached condenser, thermometer and nitrogen supply as shown in figure 4.3. The sample was heated at 140°C to facilitate solubilisation of precursors for one hour using heating mantle 500ML, Durga scientific, India. After one hour, the temperature was ramped upto boiling point of solvent for an additional hour which caused change in the color of contents from red to black. Upon cooling, excess quantity of acetone was added to precipitate the product. The precipitated product was dispersed in 20 ml toluene and sonicated. The phase transfer solution comprising of 10 ml Isopropyl alcohol+10 ml Deionised water + 1gm of KOH was added to organic phase. The product was separated by 1.5 T magnet and washed with deionised water several times till neutral pH and dispersed in deionised water for particle size analysis (11-13).

Solvothermal method of synthesis.

Phase transfer of synthesized nanoparticles.

Figure 4.3: Solvothermal process assembly and phase transfer procedure.

4.2.6. Polyol method.

4.2.6.1. Procedure.

Iron and gadolinium precursors in mole ratio of 1:10 (2.4mmol:0.24mmol) were weighed and transferred into three necked flask containing 20 ml of diol solvent (di-, tri- or tetraethylene glycol) and attached with a condenser, temperature probe (TC 513, Selec®, India) and nitrogen purge supply as shown in figure 4.4. The contents were heated to 140°C for 1 hour to facilitate the heating and stirring was done at 1000 rpm continuously using a hot plate stirrer 10MLH plus, Remi, India. After 1 hour, the temperature was ramped to 200°C for 8 hours after which the system was cooled down and the crude black liquid was washed with the washing solvent thrice. The black precipitate was dispersed in deionised water for evaluation of particle size and the remaining of the same was dried in air and stored in vials for further use as shown in figure 4.5 (14, 15).

Figure 4.4: Assembly for polyol process.

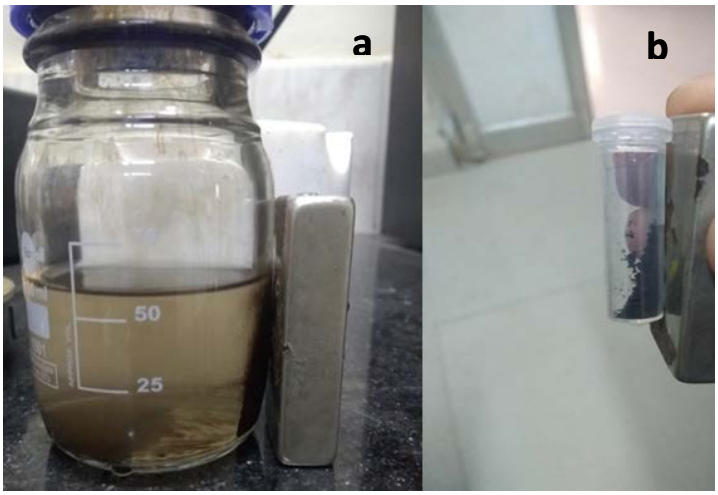

Figure 4.5: (a) Washing of crude product obtained from polyol process and (b) purified dried product of metallic nanoparticles from polyol process.

4.3. Comparison of all the methods and optimization of screened method for synthesis of metallic core.

After screening of all the methods of synthesis of Gd doped iron oxide metallic nanoparticles, the synthesis method having lowest particles size and good feasibility was selected and the reaction conditions were optimised.

4.4. Synthesis of PEI analogues.

4.4.1. Procedure.

Three analogues of PEI were synthesized namely PEI-folate (PEI-FA), PEI-triphenylphosphonium (PEI-TPP) and PEI-folate-triphenylphosphonium (PEI-FA-TPP) as scheme shown in figure 4.6. In a glass beaker, 800mg of PEI was dissolved and 200mg folic acid or 200mg (3-Carboxypropyl) triphenylphosphonium or their combination along with 200mg 1-(3-dimethylaminopropyl)-3-ethylcarbodiimide hydrochloride and 250mg N-hydroxy succinimide was dissolved in 5 ml of dimethyl sulphoxide which was added to the PEI solution. The reaction was carried out in the dark for 72 hours with constant stirring after which the resultant hazy solution was dialysed using a dialysis bag (MWCO 12000 Daltons, 2.4nm pore size) for 24 hours against double distilled water to remove the unreacted materials which was followed by lyophilisation of the PEI analogues at -60°C for 48 hours at -760mmHg using Virtis, Advantage lyophiliser, USA to get the solid product which were stored at -20°C for further use to avoid moisture uptake (16-18).

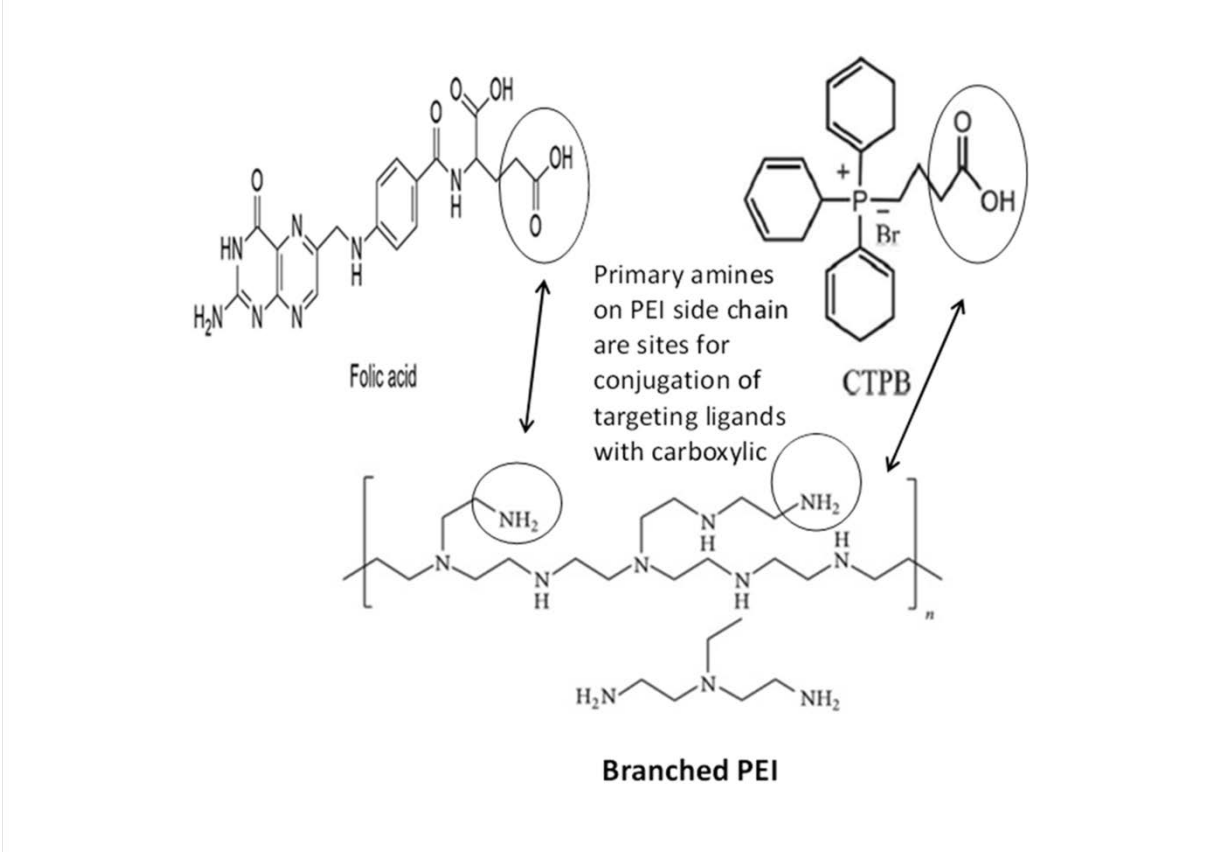

Figure 4.6: Schematic diagram of modification of PEI.

4.5. Characterization of PEI analogues.

4.5.1. Infrared spectroscopy.

The analogues of modified PEI namely PEI-FA,PEI-TPP and PEI-FA-TPP were subjected to analysis by infrared spectroscopy by using an Fourier Transform infrared spectrometer, Alpha, Bruker ,Germany (17).

4.5.2. Florescamine assay.

In different centrifuge tubes, 5 mg of modified forms were taken and 5 ml of double distilled water was added to them resulting in 1mg/ml of the solutions of modified forms of PEI. In a separate centrifuge tube florescamine solution 0.01%w/v was prepared in acetone. The standard solution of PEI(unmodified) and the test solutions were prepared as shown in table 4.1.The solutions were further diluted upto 5 ml and analysed using spectroflorimeter, RF-3501, Shimadzu, Japan with excitation wavelength of 390 nm and emission wavelength of 475 nm (19).

Table 4.1: Composition of the standard and test solutions for florescamine assay.

Solution	PEI (standard)	PEI-FA	PEI-TPP	PEI-FA-TPP
Test solution (1mg/ml)	0.1 ml	0.1 ml	0.1 ml	0.1 ml
0.1M Borate buffer pH 8	1.4 ml	1.4 ml	1.4 ml	1.4 ml
Florescamine solution 0.01% in acetone	0.5 ml	0.5 ml	0.5 ml	0.5ml
Total	2 ml	2 ml	2 ml	2 ml

4.6. Carboxylation of metallic core.

The magnetic core of Gd doped iron oxide synthesized by polyol process was taken and citric acid was added to thrice the weight of the metallic core in 10 ml deionised water and stirring was done at 1400 rpm for 72 hours for carboxylation of metallic core. After completion of the process, the magnetic core was separated by centrifugation at 10000 rpm for 10 mins using C-24 plus centrifuge, Remi, India. The washing was given with distilled water till the supernatant showed neutral pH to the pH paper (20).

4.7. Coating of drug on the metallic core and optimization.

The coating of drug lenalidomide was done on the carboxylated metallic core using nanoprecipitation technique (21). In a centrifuge tube, 5 mg of drug and Polylactide-co - glycolic acid were dissolved in 1 ml acetone which was the organic phase while the aqueous phase consisted of metallic core dispersed in 10ml polyvinyl alcohol solution. The organic phase was added into the aqueous phase rapidly under constant stirring at 2000 rpm using a magnetic stirrer. After a period of 4 hours, the evaporation of the organic phase yielded the drug coated metallic core. The surfactant concentration and the amount of PLGA were optimised to coat payload of drug and metallic core to get maximum entrapment and lowest particle size.

4.8. Secondary PEI coating on drug coated core.

Briefly, 1 ml of drug coated core was taken in a centrifugation tube and 0.5 ml of 5mg/ml solution of PEI-FA-TPP was added followed by vortexing for 1 minute. The PEI coated drug coated core is the final formulation now referred to as theranostic nanoparticles. The schematic diagram is shown in figure 4.7.

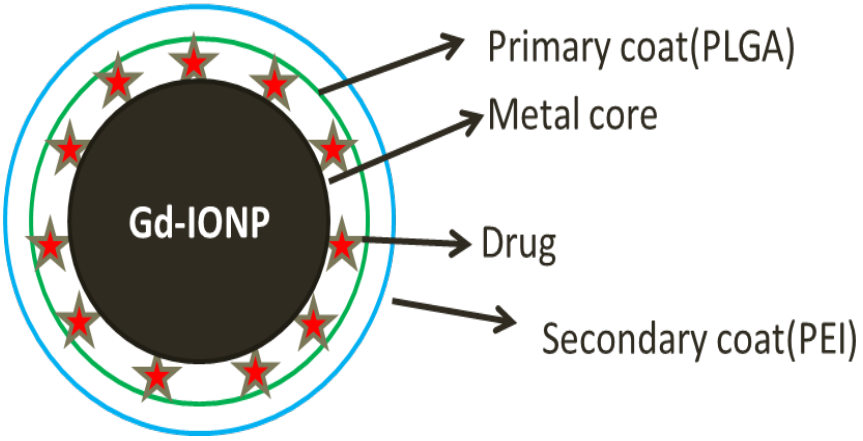

Figure 4.7: Schematic diagram of fabricated theranostic nanoparticles.

4.9. Results and discussion.

4.9.1. Screening of method for synthesis of Gadolinium doped iron oxide nanoparticles (metallic core).

There are numerous synthetic methods for synthesis of the metallic core. The selection of the method depends on many factors such as particle size and feasibility. The particle size is a critical parameter in synthesis of metallic nanoparticles as it affects the magnetic properties, biocompatibility, pharmacokinetic and toxicological profile. The smaller particle size and narrow size distribution is more preferred for clinical applications (22).

Co-precipitation is the simplest method used to synthesize metallic nanoparticles. The particle size obtained by this method was found to be 252.63±11.41 nm and polydispersity index (PDI) was 0.348±0.076 while the lowest particle size obtained was 152.66±12.84 nm with PDI of 0.140±0.010. In case of the co-precipitation method, the particle size obtained is usually polydisperse and difficult to control and also the stability is very low due to precipitation of the nanoparticles on storage. Also, larger particle size reduces the magnetization due to lesser surface area than smaller nanoparticles (23). The reaction scheme for the co-precipitation reaction is shown in figure 4.8.

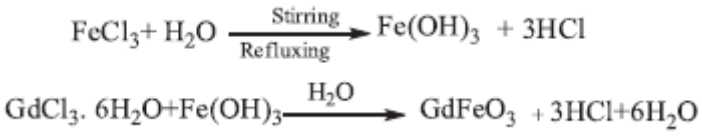

Figure 4.8: Reaction for co-precipitation synthesis (2).

The borohydride reduction method yielded the particle size of 122.86±1.96 nm with PDI of 0.375±0.018 which indicates that that particle size obtained is small but the sample is polydisperse. This can be attributed to the reaction kinetics which is difficult to control and formation of aggregates is another hurdle in synthesis (24).

Tannin synthesis or green synthesis is the method of synthesis which excludes use of toxic solvents and utilises the tannic acid which is a phytochemical obtained from plant origin (25). The reaction mechanism of the synthesis is shown in figure 4.9.The particle size obtained from the synthesis was 380.86±40.33 nm with PDI of 0.480±0.068 which indicates large particle size with polydispersity because of the spontaneous reaction.

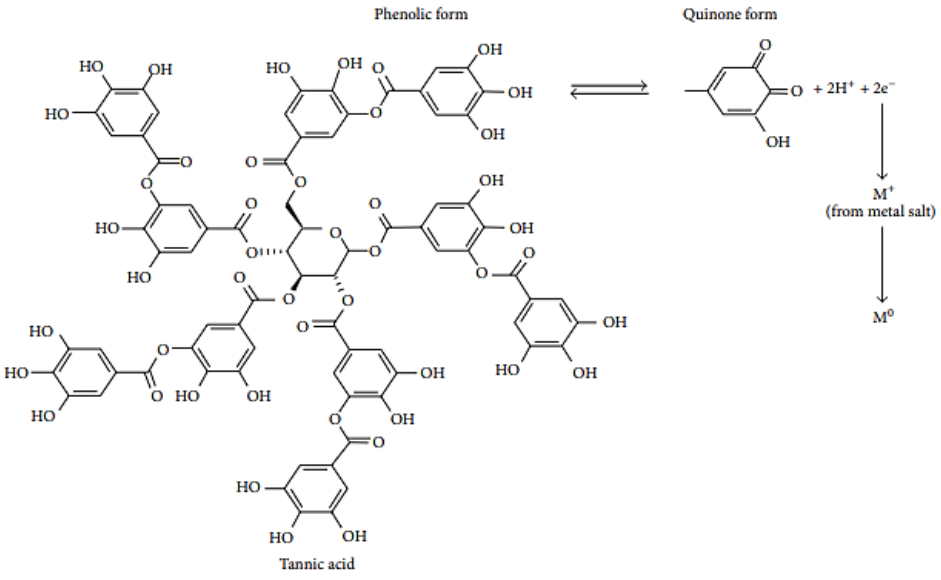

Figure 4.9: Reaction mechanism of tannin acid in synthesis of metal nanoparticles (25).

4.9.2. Determination of degradation temperature of precursors for solvothermal and polyol process.

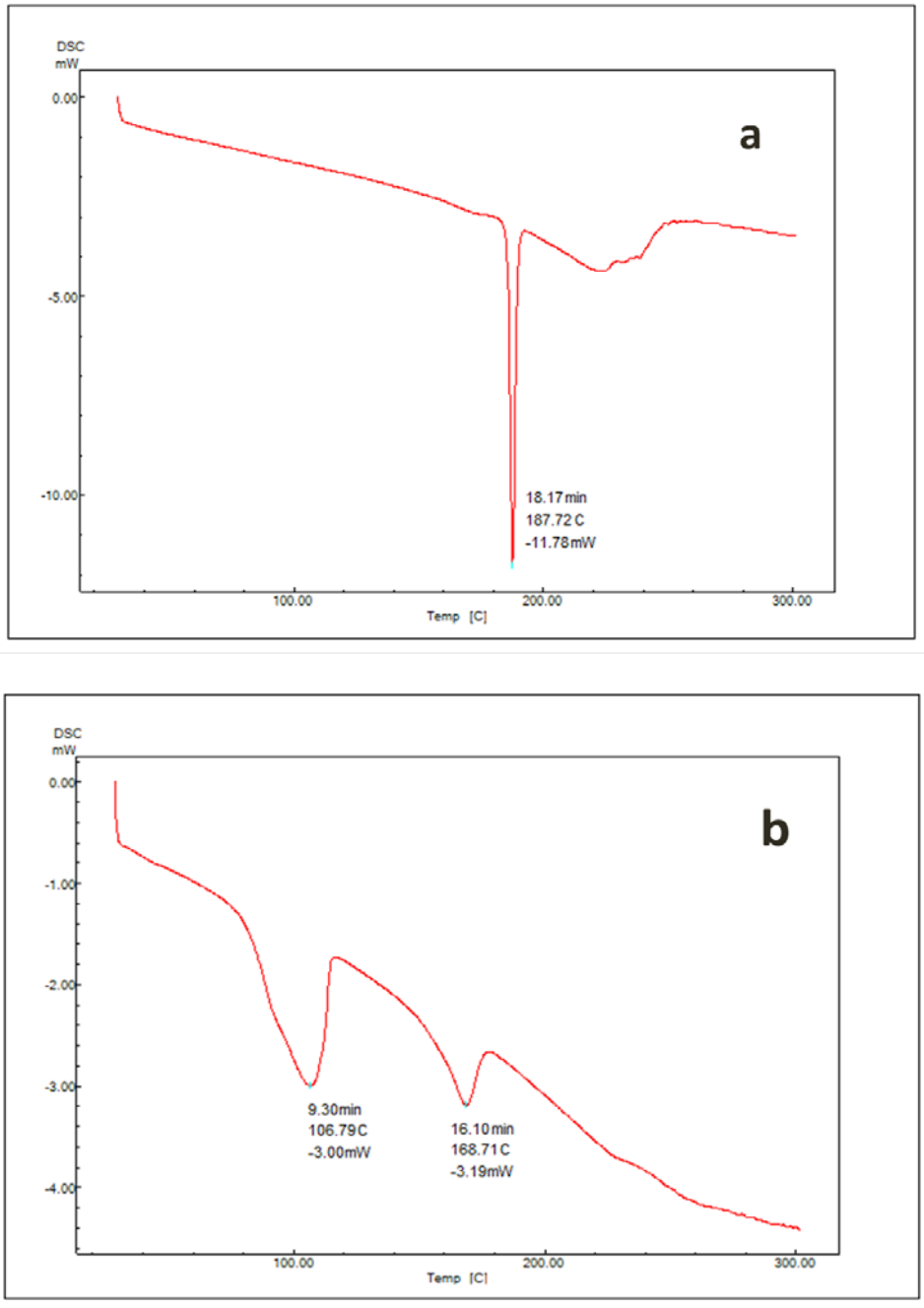

Figure 4.10: DSC thermograms of (a) Iron acetyl acetonate and (b) gadolinium acetyl acetonate hydrate.

The degradation of metallic precursors of iron and gadolinium was studied so that optimum temperature can be predicted for solvothermal and polyol process. The figure 4.10 (a) shows DSC thermogram of Iron acetylacetonate which shows a sharp endothermic peak at 187°C indicating the melting point of the compound.

After the endothermic peak there is a continuous downfall at temperature above 200°C indicating the initiation of the decomposition of the compound (26).

In case of figure 4.10 (b) there are two peaks visible for gadolinium acetyl acetonate hydrate. The first endotherm is at 106.79°C which is due to loss of water of crystallization while the second endotherm at 168.71°C is the melting point of the precursor and the continuous downfall above the melting point is indicative of the thermal decomposition if the compound (27).

4.9.3. Solvothermal method.

The solvothermal method was attempted with all the solvents using oleic acid as surfactant which yielded particles of extremely large size after phase transfer as shown in table 4.2

Table 4.2: Observations of the solvothermal method with oleic acid as surfactant.

Solvent	**Stabiliser**	**Observations**
Diphenyl ether	Oleic acid	Large particles observed after phase transfer
Benzyl ether	Oleic acid	2603 nm
Diphenyl ether	Oleic acid	Large particles observed after phase transfer
1-Octadecene	Oleic acid	Large particles observed after phase transfer

In case of oleyl amine as surfactant and 1-octadecene as the solvent the lowest particle size obtained was found to be 196.96±2.14 nm with PDI of 0.256±0.012 which indicates that the nanoparticles are polydisperse as shown in figure 4.11. The phase transfer methods can cause aggregation of nanoparticles due to incomplete removal of surfactants used in the process which can lead to increase in particle size. (28).

			Size (d.nm):	% Intensity:	St Dev (d.nm):
Z-Average (d.nm):	199.8	Peak 1:	286.7	100.0	191.2
PdI:	0.248	Peak 2:	0.000	0.0	0.000
Intercept:	0.925	Peak 3:	0.000	0.0	0.000
Result quality :	Good				

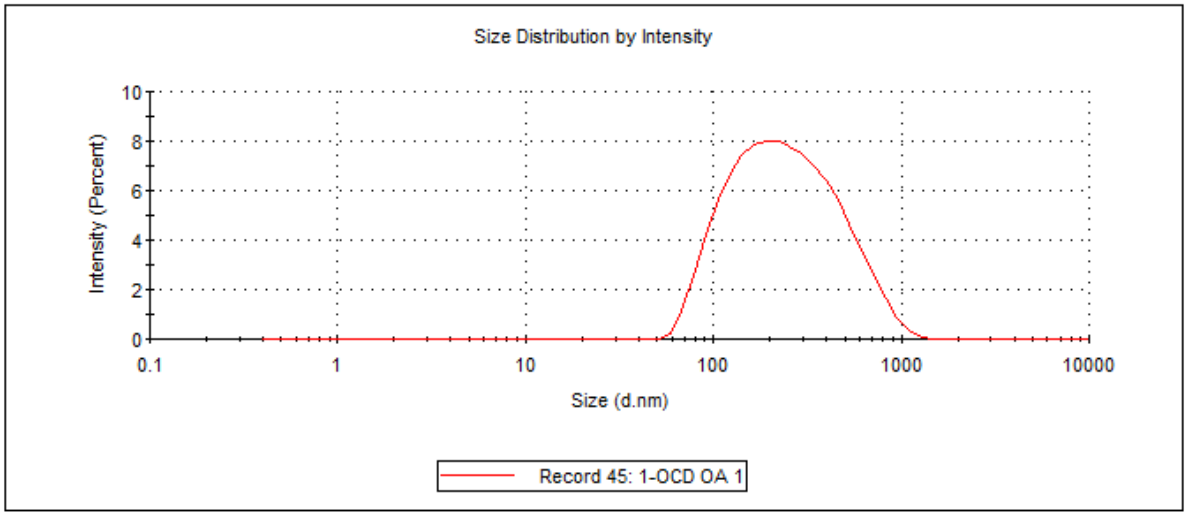

Figure 4.11: Particle size obtained in solvothermal method with oleyl amine as surfactant.

4.9.4. Polyol method.

The polyol method is a method which utilises the diols such as ethylene, diethylene, triethylene or tetraethylene glycol. The polyols have unique characteristics as they are multifunctional solvents acting as reducing agents as well as capping agents in case of synthesis of metallic nanoparticles thereby giving precise control of particle size due to colloidal stabilization. Apart from the unique characteristics of polyols, the washing step is simple due to their hydrophilicity (29). In case of the synthesis of Gd doped iron oxide nanoparticles, the solvent screening was done which revealed that tetraethylene glycol gave the magnetic product of iron oxide nanoparticles. The figure 4.12 shows the particle size obtained from the polyol method. Although the intensity distribution shows the average size of 242.4 nm in the figure the volume distribution shows peak of 12.27 nm with 89.5% volume which is due to the fact that the larger particles show more scattering of light thereby suppressing the scattering of the smaller nanoparticles in the intensity based size distribution but the volume analysis shows the particle size distribution based on the Mie's theory in which the distribution is not based on the intensity of scattered light but based on actual volume (30).

Thus it can be concluded that the particle size obtained is actually lower than the results obtained from intensity based distributions in dynamic light scattering and to confirm the actual particle size transmission electron microscopy after optimization of the reaction parameters has to be performed.

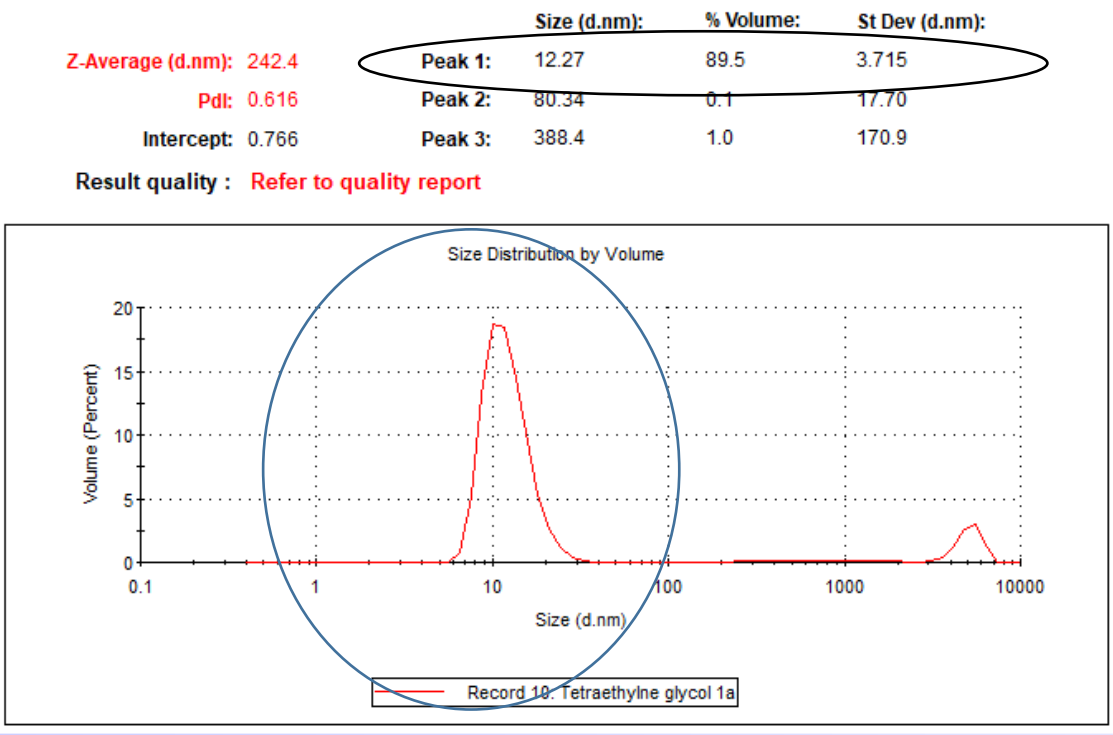

Figure 4.12: Particle size analysis of nanoparticles synthesized by polyol method.

4.9.5. Comparison of all methods for synthesis of metallic nanoparticles.

Parameter / **Method**	**Ease of synthesis**	**Particle size**	**Remarks**
Co-precipitation	Easy	Large	Single step method
Borohydride reduction	Easy	Polydisperse	Reaction is difficult to control
Tannin synthesis	Easy	Polydisperse	Method not suitable
Solvothermal	Complex method Requires caution as reaction performed at high temperatures	Large	Requires phase transfer. More suitable for synthesis in organic phase
Polyol	**Less complex than solvothermal method**	**Lowest as compared to all methods**	**Washing is easy and Single step process**

From the above facts and the results obtained from the size analysis, it can be concluded that the polyol method gave the lowest size and was optimised further for the optimum reaction conditions with lowest particle size and size distribution.

4.9.6. Optimization of Polyol method for synthesis of metallic core.

The optimization of reaction conditions for the polyol method including the temperature and reaction time were optimised as shown in table 4.3.

Table 4.3: Optimization of reaction parameters for polyol process.

a) Optimization of reaction temperature			
Batch no.	**Temperature(**°C)	**Time (hrs)**	**Size* (nm±S.D)**
1	200	8	245.43±7.93
2	250		209.86±2.73
3	300		257.66±5.70
b)Optimization of reaction time			
4	250	2	99.82±3.60
5		4	156.6±9.88
6		8	209.86±2.73
***Indicates hydrodynamic diameter n=3**			

It can be seen from table 4.3 that the reaction temperature and time have a major role on the particle size which is due to the degradation kinetics of the iron and gadolinium precursors. There is a non-linear relationship of temperature on particle size as the increase in temperature from 200°C to 250°C reduces the particle size but on further increase, there is an increase in particle size which can be due to degradation of the solvent used in process can also lead to loss of magnetic property of the metallic nanoparticles. In case of reaction time the longer reaction times increase in the particle size is due to the coalescence of the nanoparticles.

The exact mechanism of the influence of temperature and reaction time on the particle size is poorly understood (31). The optimum reaction temperature was found to be 250°C while the reaction time was found to be 2 hrs for the polyol route of synthesis of metallic core.

4.9.7. Characterization of PEI analogues.

4.9.7.1. Infrared spectroscopy.

As shown in figure 4.13 the infrared spectrum of unmodified PEI shows peaks at 3577.43 to 3020cm^{-1}(N-H stretching) due to presence of primary and secondary amine and N-H bends in the range of 1640-1550 cm^{-1} . PEI-FA, PEI-TPP and PEI-FA-TPP which are modified using carboodimide chemistry with carboxyl group containing targeting ligands - folic acid and (3-Carboxypropyl) triphenylphosphonium show peaks of amide linkage formed between primary amine of PEI and carboxylic groups of (3-Carboxypropyl) triphenylphosphonium and folic acid. In case of PEI-FA the peak is visible at 1643.97 cm^{-1}, for PEI-TPP at 1645.26 cm^{-1} and for PEI-FA-TPP at 1639.51 cm^{-1} due to formation of amide linkages. In all modified forms of PEI there is reduction in peak intensities in the region of 3577.43 to 3020cm^{-1} due to the consumption of amines in the bond formation with targeting moieties (32).

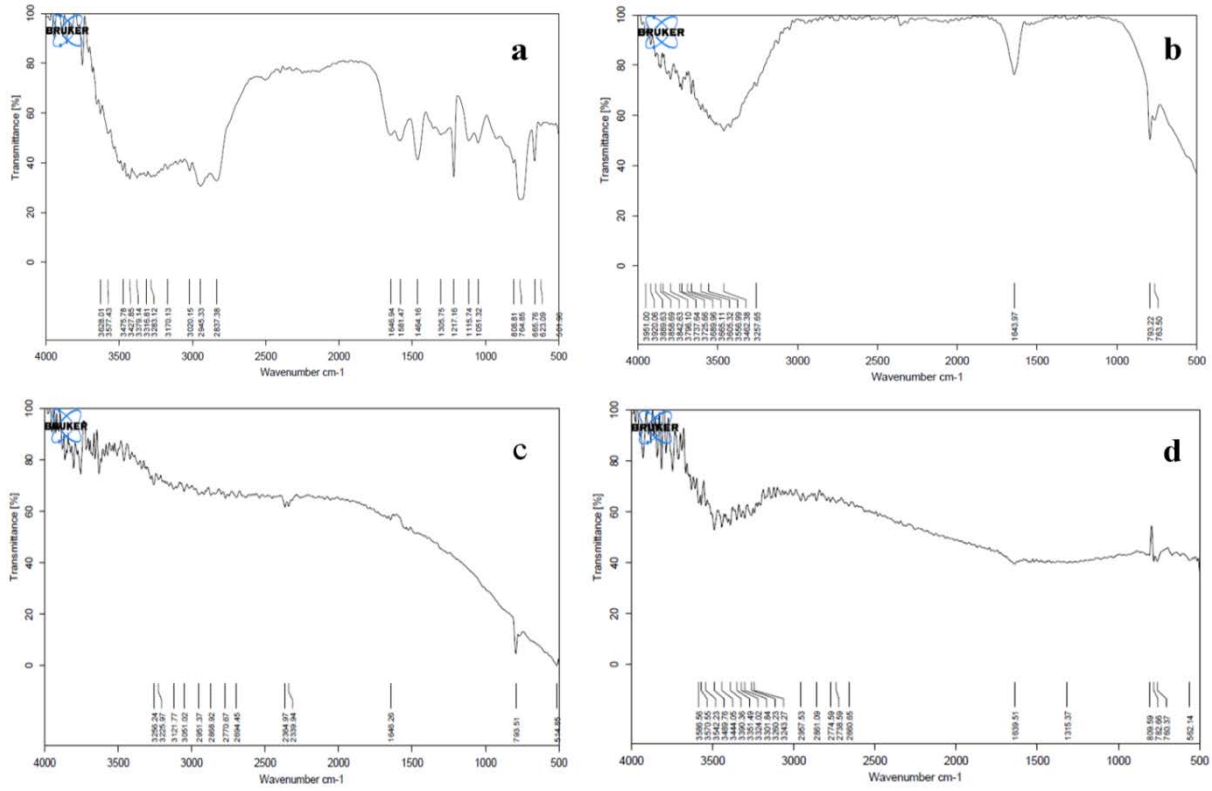

Figure 4.13: Infrared spectra of (a) PEI (b) PEI-FA (c) PEI-TPP and (d) PEI-FA-TPP.

4.9.7.2. Florescamine assay.

The working principle of florescamine assay is based on the formation of florescent product formed when the dye binds to the primary amine and shows florescence at excitation wavelength of 390nm and emission wavelength of 475nm. The higher the florescence intensity the more abundant the amine groups (33). In case of unmodified polyethylenimine (standard) there are primary amines which are free for modification giving highest florescence intensity which is used to calculate the degree of modification as per the equation given below.

$$\%Degree\ of\ modification = \frac{Florescence\ intensity\ of\ modified\ form\ of\ PEI}{Florescence\ intensity\ of\ standard\ sample\ of\ PEI} * 100$$

From the figure 4.14 it can be seen that there is reduction in the florescence intensities in all modified forms of PEI. The degree of modification of PEI-FA, PEI-TPP and PEI-FA-TPP was found to be 31.25±1.32%, 51.50±1.30% and 43.33±3.62% respectively. PEI-FA and PEI-TPP were synthesized to check the feasibility of the binding of targeting moieties with polyethylenimine. PEI-FA-TPP was used in secondary coating due to presence of dual targeting moieties.

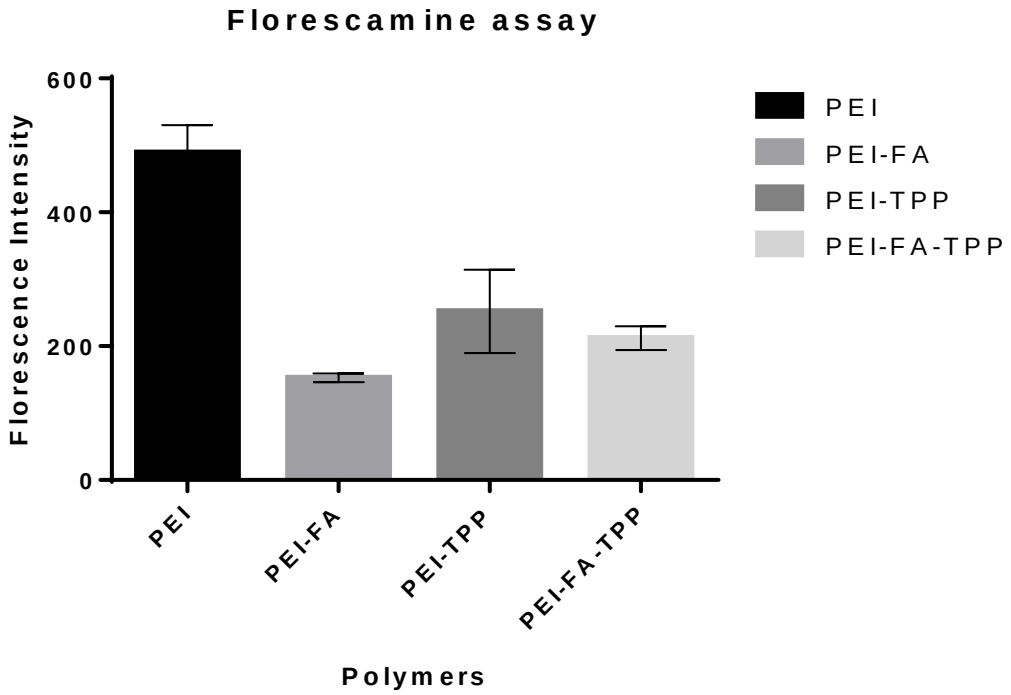

Figure 4.14: Florescamine assay for determination degree of modification of PEI (n=3).

4.9.8. Drug coating on core and its optimization.

Table 4.4 shows the optimization of drug coating to get maximum entrapment and minimum particle size using one factor at a time approach.

Table 4.4: Optimization of drug coating on metallic core.

a.) Optimization of surfactant concentration

Drug (mg)	PLGA (mg)	Drug: Polymer Ratio	Surfactant	Surfactant conc.	Size* (nm± S.D)	%EE (Average± S.D)
5	20	1:4	PVA (Mw. 6000)	0.5%	193.43±3.15	97.46±0.90
				0.8%	**185.4±2.34**	**97.61±0.61**

b.) Optimization of polymeric ratio

Drug (mg)	PLGA (mg)	Drug: Polymer Ratio	Surfactant	Surfactant conc.	Size* (nm± S.D)	%EE (Average± S.D)
5	10	1:2	PVA (Mw. 6000)	0.8%	**139.13±0.55**	**97.49±0.42**
	20	1:4			185.4±2.34	97.61±0.61

***Hydrodynamic diameter**

 # In all batches 5 mg citrate stabilised metallic core was incorporated

n=3

It can be observed from table 4.4 that the drug to polymer ratio did not have any significant effect on entrapment above the ratio of 1:2 as maximum drug entrapment was observed on that ratio which is due to the hydrophobic nature of the drug and PLGA polymer. The entrapment efficiency did not increase significantly on increasing the polymer ratio from 1:2 to 1:4, but the particle size enhancement was observed. Due to the similar hydrophobic nature of the drug and polymer, maximum partition of the drug took place in the polymer matrix of PLGA after evaporation of the organic phase which contributed to the high entrapment efficiency (34). The nanoprecipitation method was also appropriate for entrapment of lenalidomide as high entrapment of hydrophobic drugs has been reported in literature (35, 36). In case of the optimization of surfactant the amount of surfactant had significant effect on the particle size (37). The concentration <0.5% was insufficient to stabilise the nanoparticles while 0.8% of the surfactant gave the lowest particle size which is due to steric stabilization of the non-ionic polymeric chains of polyvinyl alcohol. In case of the CNS delivery of therapeutics by nanoparticles, the particle size becomes a crucial parameter as the blood brain barrier shows size dependant transport of the nanoparticles due to its anatomical characteristics (38).

4.10. References.

1. Drake P, Cho H-J, Shih P-S, Kao C-H, Lee K-F, Kuo C-H, et al. Gd-doped iron-oxide nanoparticles for tumour therapy via magnetic field hyperthermia. Journal of Materials Chemistry. 2007;17(46):4914-8.
2. Athar T, Vishwakarma SK, Bardia A, Khan AA. Super paramagnetic iron oxide and gadolinium (FeGdO3) nanopowder synthesized by hydrolytic approach passes high level of biocompatibility and MRI-based dual contrast property for competent molecular imaging and therapeutic interventions. Biomedical Physics & Engineering Express. 2016;2(2):025010.
3. Riaz S, Bashir M, Naseem S. Iron Oxide Nanoparticles Prepared by Modified Co-Precipitation Method. IEEE Transactions on Magnetics. 2014;50(1):1-4.
4. Sun J, Zhou S, Hou P, Yang Y, Weng J, Li X, et al. Synthesis and characterization of biocompatible Fe3O4 nanoparticles. Journal of biomedical materials research Part A. 2007;80(2):333-41.
5. Sun Y-P, Li X-q, Cao J, Zhang W-x, Wang HP. Characterization of zero-valent iron nanoparticles. Advances in colloid and interface science. 2006;120(1-3):47-56.
6. Zhang W-x. Nanoscale iron particles for environmental remediation: an overview. Journal of nanoparticle Research. 2003;5(3-4):323-32.
7. Sun Y-P, Li X-Q, Zhang W-X, Wang HP. A method for the preparation of stable dispersion of zero-valent iron nanoparticles. Colloids and Surfaces A: Physicochemical and Engineering Aspects. 2007;308(1-3):60-6.
8. Ruíz-Baltazar A, Esparza R, Pérez R, Rosas G. Structural Characterization of Fe-Ag Bimetallic Nanoparticles Synthesized by Chemical Reduction. International Research Journal of Pure and Applied Chemistry. 2014:263-9.
9. Herrera-Becerra R, Rius J, Zorrilla C. Tannin biosynthesis of iron oxide nanoparticles. Applied Physics A. 2010;100(2):453-9.
10. Pérez-Mirabet L, Solano E, Martínez-Julián F, Guzmán R, Arbiol J, Puig T, et al. One-pot synthesis of stable colloidal solutions of MFe2O4 nanoparticles using oleylamine as solvent and stabilizer. Materials Research Bulletin. 2013;48(3):966-72.
11. Yang H, Zhuang Y, Sun Y, Dai A, Shi X, Wu D, et al. Targeted dual-contrast T1-and T2-weighted magnetic resonance imaging of tumors using multifunctional gadolinium-labeled superparamagnetic iron oxide nanoparticles. Biomaterials. 2011;32(20):4584-93.
12. Vilas-Boas V, Guldris N, Carbó-Argibay E, Stroppa D, Cerqueira M, Espiña B, et al. Straightforward phase-transfer route to colloidal iron oxide nanoparticles for protein immobilization. RSC Advances. 2015;5(59):47954-8.
13. Xie J, Peng S, Brower N, Pourmand N, Wang SX, Sun S. One-pot synthesis of monodisperse iron oxide nanoparticles for potential biomedical applications. Pure and Applied Chemistry. 2006;78(5):1003-14.
14. Hu F, MacRenaris KW, Waters EA, Liang T, Schultz-Sikma EA, Eckermann AL, et al. Ultrasmall, water-soluble magnetite nanoparticles with high relaxivity for magnetic resonance imaging. The Journal of Physical Chemistry C. 2009;113(49):20855-60.
15. Xiao N, Gu W, Wang H, Deng Y, Shi X, Ye L. T1–T2 dual-modal MRI of brain gliomas using PEGylated Gd-doped iron oxide nanoparticles. Journal of colloid and interface science. 2014;417:159-65.
16. Wang J, Liu J. PEI–folic acid modified carbon nanodots for cancer cell-targeted delivery and two-photon excitation imaging. RSC advances. 2016;6(24):19662-8.
17. Mollarazi E, Jalilian AR, Johari-daha F, Atyabi F. Development of 153Sm-folate-polyethyleneimine-conjugated chitosan nanoparticles for targeted therapy. Journal of Labelled Compounds and Radiopharmaceuticals. 2015;58(8):327-35.
18. Huang X, Shen S, Zhang Z, Zhuang J. Cross-linked polyethylenimine–tripolyphosphate nanoparticles for gene delivery. Int J Nanomedicine. 2014;9:4785.

19. Morris VB, Sharma CP. Enhanced in-vitro transfection and biocompatibility of L-arginine modified oligo (-alkylaminosiloxanes)-graft-polyethylenimine. Biomaterials. 2010;31(33):8759-69.
20. Hachani R, Lowdell M, Birchall M, Hervault A, Mertz D, Begin-Colin S, et al. Polyol synthesis, functionalisation, and biocompatibility studies of superparamagnetic iron oxide nanoparticles as potential MRI contrast agents. Nanoscale. 2016;8(6):3278-87.
21. Prashant C, Dipak M, Yang C-T, Chuang K-H, Jun D, Feng S-S. Superparamagnetic iron oxide–Loaded poly (lactic acid)-d-α-tocopherol polyethylene glycol 1000 succinate copolymer nanoparticles as MRI contrast agent. Biomaterials. 2010;31(21):5588-97.
22. Xie W, Guo Z, Gao F, Gao Q, Wang D, Liaw B-S, et al. Shape-, size- and structure-controlled synthesis and biocompatibility of iron oxide nanoparticles for magnetic theranostics. Theranostics. 2018;8(12):3284-307. PubMed PMID: 29930730. eng.
23. Wu W, He Q, Jiang C. Magnetic iron oxide nanoparticles: synthesis and surface functionalization strategies. Nanoscale research letters. 2008;3(11):397-415.
24. Vernaya O, Peisikova A, Fuki M, Shabatin V, Shabatina T. Effect of the Conditions the Reaction on the Formation of Iron Nanoparticles during the Reduction of Iron (III) Ions with Sodium Borohydride. Moscow University Chemistry Bulletin. 2019;74(6):326-9.
25. Ahmad T. Reviewing the tannic acid mediated synthesis of metal nanoparticles. Journal of Nanotechnology. 2014;2014.
26. Haham H, Grinblat J, Sougrati M-T, Stievano L, Margel S. Engineering of iron-based magnetic activated carbon fabrics for environmental remediation. Materials. 2015;8(7):4593-607.
27. Lv F, Zhang Y, Chen X, Ma Y. Composition and Fluorescence of Gadolinium (III) Acetyl-acetonate Derivatives by Solvothermal Method. Int J Opt Photonics Eng. 2017;2.
28. Cai J, Miao YQ, Yu BZ, Ma P, Li L, Fan HM. Large-scale, facile transfer of oleic acid-stabilized iron oxide nanoparticles to the aqueous phase for biological applications. Langmuir. 2017;33(7):1662-9.
29. Dong H, Chen Y-C, Feldmann C. Polyol synthesis of nanoparticles: status and options regarding metals, oxides, chalcogenides, and non-metal elements. Green chemistry. 2015;17(8):4107-32.
30. Stetefeld J, McKenna SA, Patel TR. Dynamic light scattering: a practical guide and applications in biomedical sciences. Biophysical reviews. 2016;8(4):409-27.
31. Cheng C, Xu F, Gu H. Facile synthesis and morphology evolution of magnetic iron oxide nanoparticles in different polyol processes. New Journal of Chemistry. 2011;35(5):1072-9.
32. Arabi S, Akbari Javar H, Khoobi M. Preparation and characterization of modified polyethyleneimine magnetic nanoparticles for cancer drug delivery. Journal of Nanomaterials. 2016;2016.
33. Derayea SM, Samir I. A review on the use of fluorescamine as versatile and convenient analytical probe. Microchemical Journal. 2020;156:104835.
34. Wischke C, Schwendeman SP. Principles of encapsulating hydrophobic drugs in PLA/PLGA microparticles. International Journal of pharmaceutics. 2008;364(2):298-327.
35. Jani P, Vanza J, Pandya N, Tandel H. Formulation of polymeric nanoparticles of antidepressant drug for intranasal delivery. Therapeutic delivery. 2019;10(11):683-96.
36. Liu Y, Yang G, Zou D, Hui Y, Nigam K, Middelberg APJ, et al. Formulation of Nanoparticles Using Mixing-Induced Nanoprecipitation for Drug Delivery. Industrial & Engineering Chemistry Research. 2020 2020/03/04;59(9):4134-49.
37. Martínez Rivas CJ, Tarhini M, Badri W, Miladi K, Greige-Gerges H, Nazari QA, et al. Nanoprecipitation process: From encapsulation to drug delivery. International Journal of Pharmaceutics. 2017 2017/10/30/;532(1):66-81.
38. Nowak M, Brown TD, Graham A, Helgeson ME, Mitragotri S. Size, shape, and flexibility influence nanoparticle transport across brain endothelium under flow. Bioengineering & translational medicine. 2020;5(2):e10153.